Two impurities in a *d*-wave superconductor: Local density of states

Lingyin Zhu,[1] W. A. Atkinson,[2,1] and P. J. Hirschfeld[1,3]
[1]*Department of Physics, University of Florida, Gainesville, Florida 32611*
[2]*Department of Physics, Southern Illinois University, Carbondale, Illinois 62901-4401*
[3]*Center for Electronic Correlations and Magnetism, EP6, University Augsburg, Augsburg, Germany*
(Received 31 July 2002; revised manuscript received 14 November 2002; published 20 March 2003)

We study the problem of two local potential scatterers in a *d*-wave superconductor, and show how quasiparticle bound-state wave functions interfere. Each single-impurity electron and hole resonance energy is in general split in the presence of a second impurity into two, corresponding to one even parity and one odd parity state. We calculate the local density of states (LDOS), and argue that scanning tunneling microscopy (STM) measurements of two-impurity configurations should provide more robust information about the superconducting state than one-impurity LDOS patterns. In some configurations highly localized, long-lived states are predicted. We discuss the effects of realistic band structures, and how two-impurity STM measurements could help distinguish between current explanations of LDOS impurity spectra in the BSCCO-2212 system.

DOI: 10.1103/PhysRevB.67.094508 PACS number(s): 74.25.Bt, 74.25.Jb, 74.40.+k

I. INTRODUCTION

The study of isolated pointlike impurities in *d*-wave superconductors began with the observation that the scattered wave pattern probed in tunneling experiments should inherit the fourfold symmetry of the *d*-wave state.[1] It was pointed out shortly afterwards by Salkola *et al.*,[2] following earlier work on the analogous *p*-wave problem by Stamp,[3] that quasibound resonances should occur near strongly scattering impurities. Both the resonance energy and the details of the spatial structure of the resonant wave pattern depend sensitively on electron correlations and a large body of theoretical work exists exploring this relationship.[4] Assuming that the important details of the scattering potential are understood, careful studies of the local density of states (LDOS) near isolated impurites provide a uniquely powerful probe of the superconducting state. Experimentally, the high-temperature superconductors, notably $Bi_2Sr_2CaCu_2O_{8+\delta}$ (BSCCO), have been examined with sensitive scanning tunneling microscopy (STM) techniques. Images of the local environment of impurities[5,6] have confirmed the existence of quasi-bound states near strongly scattering impurities like Zn, but have led to new questions regarding the microscopic model for impurities and the superconducting state itself.

Other types of inhomogeneities not directly correlated with impurity resonances have been discovered by STM measurements on the cuprates. These include the observation of large, quasibimodal nanoscale fluctuations of the superconducting order parameter, together with spatially correlated variations of the electronic structure and lifetime.[7,8] More recently, the observation of checkerboard patterns in the LDOS of vortex cores[9] and in inhomogeneous samples in zero field[10] in BSCCO has led to speculation that antiferromagnetic phases can be formed in regions where superconductivity is supressed.[11] A good deal of subsequent theoretical work on the competition between *d*-wave superconductivity and various exotic order parameters[12] has excited the high-T_c community with the suggestion that STM measurements could be revealing the presence of competing magnetic or other exotic subdominant order, shedding light on the origins of superconductivity itself.

On the other hand, a more conventional but still fascinating explanation has been put forward by Hoffman *et al.*,[13] who argue that Friedel oscillations related to quasiparticle scattering between nearly parallel sections of the Fermi surface can lead to the observed checkerboard patterns, which correspond to well-defined dynamical peaks in momentum space. These general remarks were followed very recently by a calculation by Wang and Lee[14] studying the Friedel oscillations of a single impurity in a *d*-wave superconductor in momentum space. These calculations support the idea that what STM is seeing is primarily the effect of quasiparticle wave functions interfering with one another in a fluctuating disorder field on a *d*-wave superconducting background.

Studies of true *interference* of quasiparticle wave functions in the presence of more than a single impurity are rare, however. Numerical solutions of the many-impurity problem yield little insight into the mechanism of interference itself. In principle, the problem of two impurities is the simplest one which displays the interference effects of interest for the present problem; we study it here in order to understand whether the STM analysis of isolated impurity resonances is indeed justified, and to test if the scenario proposed by Hoffman *et al.*[13] is tenable in the presence of interfering Friedel oscillations. There is a small amount of earlier work on two impurities in a *d*-wave superconductor, most of it also numerical. Onishi *et al.*[15] solved the Bogoliubov-de Gennes (BdG) equations and presented a few local density of states profiles for two impurities. In a work philosophically related to ours, the interference of bound-state wave functions in the fully disordered system was discussed by Balatsky in the context of supression of localization effects due to impurity band formation.[16] Micheluchi and Kampf have recently exhibited numerically how impurity induced bound states accumulate at low energies, and argued that the impurity band at low energies could be studied from this perspective.[17] Finally, during the preparation of this manuscript, a paper by Morr and Stavropoulos examined the two-impurity problem with particular emphasis on predictions for cuprate STM

studies.[18] We comment throughout the text on comparisons with these previous works.

We begin in Sec. II by reviewing the solution to the single-impurity problem which has been studied by several authors. In Sec. III, we setup the formalism for the two-impurity problem and give the exact solution for the *T*-matrix, as well as a simplified form for some special cases. In Sec. IV, we discuss the dependence of the resonance splittings on the orientation and magnitude of the interimpurity separation **R**. The resonant energy splittings are argued to give important information which is qualitatively different from that is obtainable from one-impurity resonance energies; in particular, they allow one, in principle, to map out, by repeated measurements of energies for impurity configurations at separation **R**, the spatial structure of the homogeneous superconducting Green's function. Starting from two widely separated impurities with $R \gg \xi_0$, where ξ_0 is the coherence length, we then give analytical solutions for the splittings which exhibit explicitly the strong dependence on the direction of **R** due to the *d*-wave nodes. Impurities located along a 100 axis interact very weakly for $R \gtrsim \xi_0$, whereas configurations near 110 relative orientation lead to strong hybridization.

In Sec. V, we begin by discussing the simple quantum-mechanics problem of how bound eigenstates with two scattering centers are constructed from the eigenstates of one, and show how these states may be classified. Of four states which arise from the single-impurity particle and hole resonances, two are spatially symmetric (s), and two antisymmetric (p), one on each side of the Fermi level. The energy ordering of these states, as well as the crude qualitative interference pattern (constructive or destructive) depends on the configuration **R** in a predictable way. The local density of states is then calculated and plotted for several cases to illustrate the spatial dependence of the resonant state wave functions. Spectra on individual sites reveal unexpected phenomena: in certain circumstances the one-impurity states, which become sharper as they approach the Fermi level due to the coupling to the linear *d*-wave continuum, interfere to create localized, extremely sharp states located at energies quite far from the Fermi level. In Sec. VI we discuss the situation for a more realistic band characteristic of the BSCCO-2212 system on which impurity STM studies have been performed. The trapped quasiparticle states are still found, and a dynamical resonanance criterion depending on the exact Fermi surface and impurity orientation **R** is identified.

Finally, in Sec. VII we present our conclusions and discuss the implications for STM experiments and other aspects of the disordered quasiparticle problem.

II. SINGLE-IMPURITY PROBLEM

In broad terms, there are two distinct points of view which have evolved regarding the localized scattering resonances observed by STM on the surface of BSCCO-2212. In the traditional quasiparticle picture, one simply calculates the scattering *T*-matrix for noninteracting BCS quasiparticles in a *d*-wave superconductor and finds a pair of resonances which are approximately symmetric in energy about the Fermi level, and which have distinctive spatial patterns.[4] In the second point of view, additional physics arises from the local disruption of the strongly correlated ground state by the impurity which is predicted to break singlet correlations,[19,20] nucleate short-ranged antiferromagnetic order,[21–26] or spin fluctuations associated with a nearby phase transition.[18,27] Perhaps the strongest motivation for this point of view is the observation of local moments near Li and Zn impurities in the superconducting state of underdoped yttrium barium copper oxide (YBCO), as observed in NMR[28,29] experiments. For the STM experiments, the basic question is whether the spatial structure which is observed at low energies is effectively the result of BCS quasiparticles scattering from a short-range potential (i.e., Friedel oscillations), or requires consideration of local correlation effects (e.g., spin-density wave formation[27]) or dynamical effects (Kondo physics).[19,30]

One notable feature of the STM experiments on Zn-doped samples of BSCCO is that only a single, negative-energy resonance with a resonance energy of ≈ -1.5 meV is seen;[6] the predicted impurity-induced resonances come in mirror pairs as a consequence of the particle-hole symmetry of the superconducting state. A further inconsistency is the fact that a large LDOS is observed on the Zn impurity site; the strong repulsive potential which Zn is believed to possess must necessarily allow little or no electron spectral weight at the impurity site. One appealing explanation[31,32] is that the measured LDOS of the CuO_2 planes is in fact *filtered* by an inert surface layer, leading to an apparent redistribution of spectral weight in the tunneling LDOS. With this mechanism, one can simply understand the LDOS without introducing strong correlation physics. We note, however, that while this mechanism explains the observed LDOS for Zn impurities, it is problematic for both Ni impurities and Cu vacancies, which are consistent with the quasiparticle picture without invoking a filtering mechanism. (To date, there is no convincing model which has explained the spatial distribution of the LDOS in all three cases.) One of the goals of this work is to study the effect of the filtering mechanism on the resonant structure of two closely spaced strongly scattering impurities within the quasiparticle point of view, providing a more rigorous test of the quasi-particle-plus-filter mechanism for Zn impurities.

The BCS Hamiltonian for a pure singlet superconductor can be written as

$$H_0 = \sum_{\mathbf{k}} \Phi_{\mathbf{k}}^{\dagger} (\epsilon_{\mathbf{k}} \tau_3 + \Delta_k \tau_1) \Phi_{\mathbf{k}}, \tag{1}$$

where $\Phi_{\mathbf{k}} = (c_{\mathbf{k}\downarrow} c_{-\mathbf{k}\uparrow}^{\dagger})$, is a Nambu spinor. In this work we will consider several forms for the dispersion $\epsilon_{\mathbf{k}}$. Analytic results are presented for a parabolic band $\epsilon_{\mathbf{k}} = k^2/2m$, with corresponding *d*-wave order parameter $\Delta_{\mathbf{k}} = \Delta_{max} \cos 2\phi$ (ϕ is the angle in momentum space which **k** makes with the 100 axis). Numerical results are presented for a simple tight-binding model $\epsilon_{\mathbf{k}} = -2t(\cos k_x + \cos k_y) - \mu$ and for a realistic six-parameter tight-binding model proposed by Norman *et al.*,[33] both having the corresponding *d*-wave order parameter $\Delta_{\mathbf{k}} = \Delta_0(\cos k_x - \cos k_y)$. Note the maximum value of the

order parameter in the lattice system with the current convention is $2\Delta_0$. The matrices τ_i are the Pauli matrices.

The Hamiltonian of a single on-site impurity at $\mathbf{r}=0$ may be written as $H_{imp}=\Sigma_{\mathbf{k},\mathbf{k}'}V_0\Phi_{\mathbf{k}}^{\dagger}\tau_3\Phi_{\mathbf{k}'}$, where V_0 is the strength of the impurity potential. The Green's function $\hat{G}_{\mathbf{k}\mathbf{k}'}(\omega)$ in the presence of the impurity is expressed in terms of Green's function $\hat{G}_{\mathbf{k}}^0(\omega)$ for the pure system as $\hat{G}(\mathbf{k},\mathbf{k}',\omega)=\hat{G}^0(\mathbf{k},\omega)\delta_{\mathbf{k}\mathbf{k}'}+\hat{G}^0(\mathbf{k},\omega)\hat{T}(\omega)\hat{G}^0(\mathbf{k}',\omega)$, where the $\hat{}$ symbol indicates a matrix in Nambu space. The solution is

$$\hat{T}=T_0\tau_0+T_3\tau_3,$$

$$T_0=V_0^2G_0/(S_+S_-),$$

$$T_3=V_0^2(c-G_3)/(S_+S_-), \tag{2}$$

where G_0 and G_3 are the τ_0 and τ_3 Nambu components of the integrated bare Green's function $\Sigma_{\mathbf{k}}\hat{G}^0(\mathbf{k},\omega)$. This expression has resonances when

$$S_{\pm}\equiv 1-V_0(G_3\mp G_0)=0. \tag{3}$$

Note that in a simple band $1/(\pi N_0V_0)\equiv c/(\pi N_0)$ is the cotangent of the *s*-wave scattering phase shift η_0, where N_0 is the density of states at the Fermi level. In the special case of a particle-hole symmetric system, $G_3=0$ and the resonance energy is determined entirely by G_0, which is given in the case of a circular Fermi surface by $G_0(\omega)=-i\int(d\varphi/2\pi)\omega[\omega^2-\Delta_{\mathbf{k}}^2]^{-1/2}$ which for low energies $\omega\ll\Delta_{max}$ takes the form $G_0(\omega)\simeq-(\pi\omega/\Delta_{max})(\ln 4\Delta_{max}/\omega+i)$. One may then solve Re $S_{\pm}(\omega+i0^+)=0$ and estimate the resonance width Γ on the real axis. In the case of strong scattering $c\ll N_0$, the resonance energy $\Omega_0^{\pm}$ and scattering rate Γ are

$$\Omega_0^{\pm}=\frac{\pm\pi c\Delta_0}{2\ln(8/\pi c)} \tag{4a}$$

$$\Gamma=\frac{\pi^2c\Delta_0}{4\ln^2(8/\pi c)}. \tag{4b}$$

This result was first obtained by Balatsky *et al.*,[2] following earlier work on the *p*-wave analog problem by Stamp.[3] Note that the resonance becomes a true bound state only exactly at the Fermi level $\Omega=0$, when $c=0$; for finite c there are two resonances whose energies are symmetric, $\Omega_0^+=-\Omega_0^-$ in this approximation. As seen from Eq. (3), in particle-hole asymmetric systems ($G_3\neq 0$), the resonance is tuned to sit at the Fermi level for some value of the impurity potential V_0 which is not infinite, so the term "unitarity" (as used in this work, $\Omega_0=0$) and "strong potential" ($V_0\to\infty$) are not synonymous.[34,36]

The ambiguity in defining the resonance energy precisely arises already at the level of the one-impurity problem. Equation (3) is in fact an equation for a complex frequency ω, which may be shown to have no solution in the upper half plane. Thus the T matrix has no true pole at any $\omega=\Omega'+i\Omega''$ in the complex plane, but only a maximum which lies along the real axis. Only when the real part Ω' approaches the Fermi level does the damping become sufficiently small to allow one to speak of a well-defined resonance in this case the real part Ω' approaches the solution $\Omega_0^{\pm}$ of Re$[S_{\pm}]=0$ for ω on the real axis. For this reason the "resonance energy" is usually taken to be $\Omega_0^{\pm}$, as given, e.g., in Eq. (4a) for the particle-hole symmetric case. It is important to keep in mind, however, that the definition becomes meaningless as the bound-state energy moves far from the Fermi level; for example, the apparent divergence of Eq. (4a) as $c\to 8/\pi$ is artificial, since no well-defined resonant state exists by the time Ω_0 is a significant fraction of the gap Δ_0. It should also be noted that the generalization of this resonance criterion to more complicated situations, where the denominator does not factor, is not straightforward.

Even if the *energies* of the particle and hole resonant states are symmetric, their *spectral weights* on a given site may be quite different.[2,4] The finite impurity potential acts as a local breaker of particle-hole symmetry, leading in the case of repulsive potential to a large peak in $\rho(\mathbf{r},\omega)$ at the impurity site $\mathbf{r}=0$ at negative energy(holelike states) and a small feature at positive energy (electronlike), as seen in Fig. 1. The impurity-induced LDOS decays as r^{-2} along the nodal directions (for the particle-hole symmetric system), and exponentially along the antinodes. The LDOS in the near field is more complicated, however: the nearest-neighbor sites have peaks at $\pm\Omega_0$, with the larger spectral weight at $+\Omega_0$. In the crossover regime $r\sim\xi_0$, the LDOS is enhanced along the node direction for holelike states, but is spread perpendicular to the node direction for electronlike states. These spatially extended LDOS patterns are the fingerprint of the impurity-induced virtual bound states. In Fig. 1, we illustrate the LDOS pattern expected for both particles and holes for a resonant state close to the Fermi level. Results are obtained with a simple half-filled tight-binding band, $\epsilon_{\mathbf{k}}=-2t(\cos k_x+\cos k_y)$, and unless otherwise specified all energies are given in units of the hopping t.

At the present writing, the LDOS pattern produced within the simple T-matrix theory for a single strong impurity, while fourfold in symmetry, does not agree in detail with STM experiments on Zn impurities and native planar defects.[6] It is not currently clear whether this is due to a failing of the microscopic impurity model, e.g., failure to include strong correlations in the host or magnetic degrees of freedom or whether a relatively trivial tunneling matrix element effect prevents direct observation of the simple pattern by STM. For the moment then we consider only the simplest two-impurity model possible, recognizing that direct application to experiments awaits a resolution of the discrepancy at the one-impurity level.

III. *T* MATRIX FOR TWO IMPURITIES

We now introduce the formalism necessary to study the interference between two resonances of the type discussed above when two identical impurities are brought close to one another. The perturbation due to two identical impurities located at positions $\mathbf{R}_l$ and $\mathbf{R}_m$, is given by

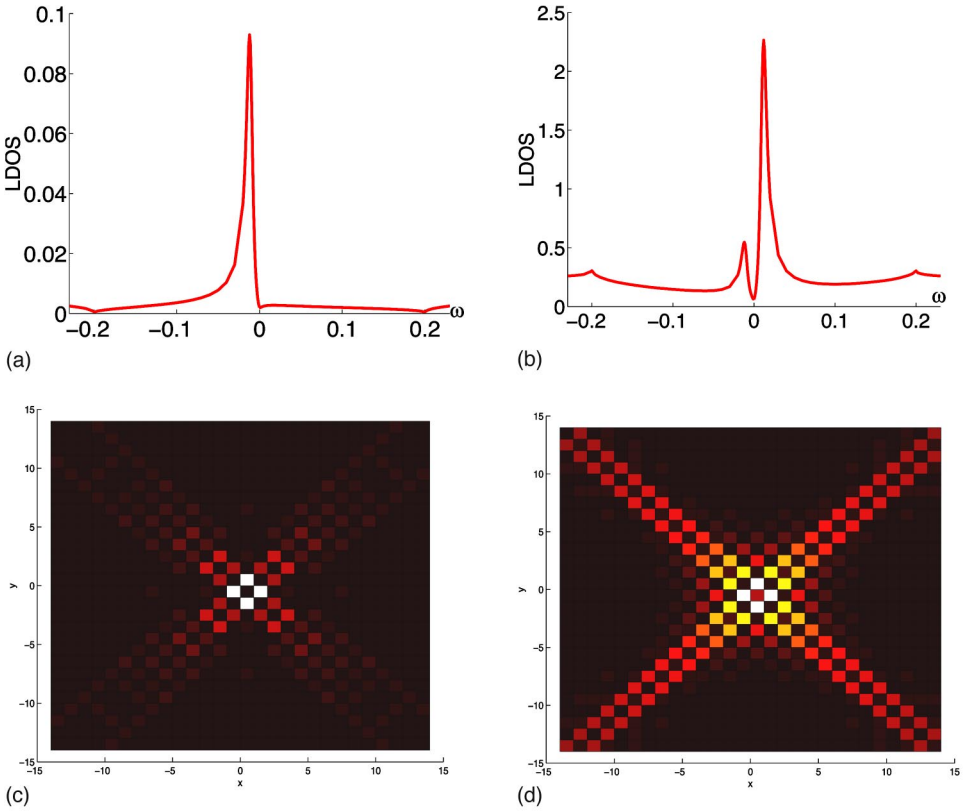

FIG. 1. (Color online) Summary of LDOS results for one-impurity problem on a tight-binding lattice, $\Delta_0=0.1$, $\mu=0, V_0=10$, $|\Omega_0^{\pm}|\simeq 0.013$: (a) LDOS vs ω on the impurity site; (b) LDOS vs ω on nearest-neighbor site; (c),(d) LDOS map at resonance $\omega=\Omega_0^+$ and $\omega=\Omega_0^-$. Color scales in (c) and (d) are relative to the nearest-neighbor peak heights shown in (b).

$$\hat{H}_{imp}=V_0\sum_{i=l,m}\mathbf{\Phi}_i^{\dagger}\tau_3\mathbf{\Phi}_i, \tag{5}$$

where $\mathbf{\Phi}_i\equiv[c_{i\uparrow}^{\dagger}c_{i\downarrow}]$. By iterating the procedure for the single-impurity T matrix with two impurities present we find, in a 4×4 basis of spin and impurity site labels,[37]

$$\hat{T}_{lm}(\omega)=\begin{pmatrix}\hat{f}\hat{T}_l & \hat{f}\hat{T}_l\hat{G}^0(\mathbf{R})\hat{T}_m\\ \hat{f}\hat{T}_m\hat{G}^0(-\mathbf{R})\hat{T}_l & \hat{f}\hat{T}_m\end{pmatrix}, \tag{6}$$

where $\mathbf{R}=\mathbf{R}_l-\mathbf{R}_m$ and where $\hat{T}_l,\hat{T}_m$ are the single-impurity T matrices associated with the two impurities. For identical impurities, $\hat{T}_l=\hat{T}_m=\hat{T}(\omega)$, the single-impurity T matrix defined previously. The quantity $\hat{f}$ is defined as

$$\hat{f}(\omega)=[1-\hat{G}^0(-\mathbf{R},\omega)\hat{T}_l(\omega)\hat{G}^0(\mathbf{R},\omega)\hat{T}_m(\omega)]^{-1}, \tag{7}$$

where $\hat{G}^0(\mathbf{R},\omega)=\Sigma_{\mathbf{k}}\exp[i\mathbf{k}\cdot\mathbf{R}]G_{\mathbf{k}}^0(\omega)$ is just the Fourier transformation of $\hat{G}_{\mathbf{k}}^0(\omega)$, the unperturbed Nambu Green's function. For systems with inversion symmetry $\hat{G}^0(\mathbf{R},\omega)=\hat{G}^0(-\mathbf{R},\omega)$. Note that in Eq. (6), the physical processes are clearly identifiable as multiple scatterings from each impurity l and m individually, plus interference terms where electrons scatter many times between l and m. In $\mathbf{k}$ space, we can write the T matrix in the more usual 2×2 notation as

$$\hat{T}_{\mathbf{k}\mathbf{k}'}(\omega)=[e^{i\mathbf{k}\cdot\mathbf{R}_l}\tau_0e^{i\mathbf{k}\cdot\mathbf{R}_m}\tau_0]\hat{T}_{lm}\begin{bmatrix}e^{-i\mathbf{k}'\cdot\mathbf{R}_l}\tau_0\\ e^{-i\mathbf{k}'\cdot\mathbf{R}_m}\tau_0\end{bmatrix}, \tag{8}$$

where τ_0 is the Pauli matrix. In Sec. II we showed that, provided the resonance energies are distinct, peaks in the total density of states correspond to minima of the T-matrix denominator,

$$\mathcal{D}\equiv\det[1-\hat{G}^0(-\mathbf{R},\omega)\hat{T}(\omega)\hat{G}^0(\mathbf{R},\omega)\hat{T}(\omega)]. \tag{9}$$

Explicitly, $\mathcal{D}=\mathcal{D}_1\mathcal{D}_2/(S_+^2S_-^2)$ with

$$\mathcal{D}_1=\mathcal{D}_1^+\mathcal{D}_1^-+V_0^2G_1^2(\mathbf{R},\omega),$$
$$\mathcal{D}_2=\mathcal{D}_2^+\mathcal{D}_2^-+V_0^2G_1^2(\mathbf{R},\omega), \tag{10}$$

where

$$\mathcal{D}_{\alpha}^{\pm}=[1-V_0G_3(0,\omega)\pm V_0G_0(0,\omega)]$$
$$+(-1)^{\alpha}V_0[\mp G_0(\mathbf{R},\omega)+G_3(\mathbf{R},\omega)]. \tag{11}$$

The factors $\mathcal{D}_1,\mathcal{D}_2$ determine the four two-impurity resonant energies. Here $G_{\alpha}(\mathbf{R},\omega)$ is the τ_{α} component of the integrated bare Green's function

$$G_{\alpha}(\mathbf{R},\omega)=\frac{1}{2}\mathrm{Tr}(\tau_{\alpha}G^0(\mathbf{R},\omega)). \tag{12}$$

For completeness, we also give the explicit form of the T matrix itself,

$$\hat{T}_{\mathbf{k},\mathbf{k}'}(\omega)=\frac{2V_0}{\mathcal{D}_1\mathcal{D}_2}[\cos(\mathbf{k}\cdot\mathbf{R}/2)\cos(\mathbf{k}'\cdot\mathbf{R}/2)\hat{M}_s(\omega)$$
$$+\sin(\mathbf{k}\cdot\mathbf{R}/2)\sin(\mathbf{k}'\cdot\mathbf{R}/2)\hat{M}_p(\omega)], \tag{13}$$

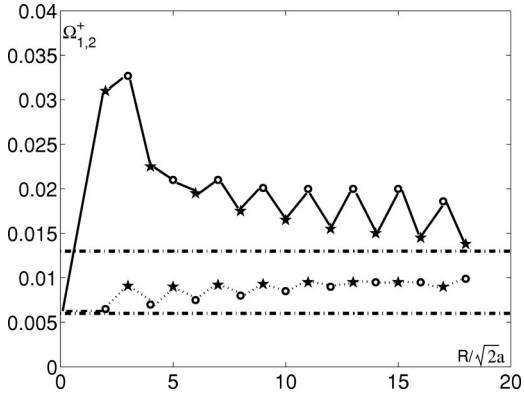

FIG. 2. Two-impurity resonance energies $\Omega^+_{1,2}>0$ vs impurity separation $R/(\sqrt{2}a)$ for $\mathbf{R}\|(110)$, $\mu=0$, $\Delta_0=0.1$, $V_0=10$. Solid line, upper two-impurity positive resonance energy; dashed line, lower two-impurity resonance energy; upper dashed-dotted line, reference one-impurity resonance energy $\Omega^+_0(V_0)$. Lower dashed-dotted line, one-impurity resonance energy for double-impurity strength $\Omega^+_0(2V_0)$. Symbol indicates resonant channel, $\circ=\Omega^+_1>0$; $\star=\Omega^+_2>0$.

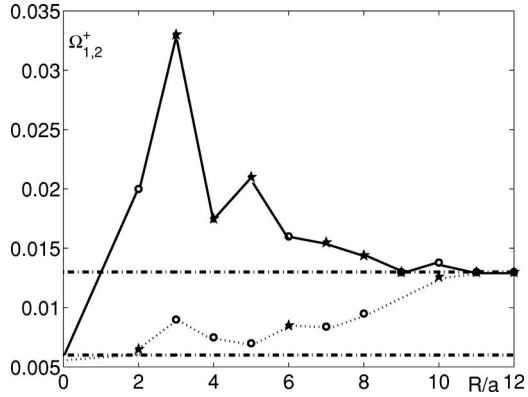

FIG. 3. Two-impurity resonance energies $\Omega^+_{1,2}/t>0$ vs impurity separation $R/(a)$ for $\mathbf{R}\|(100)$, $\mu=0$, $\Delta_0=0.1$, $V_0=10$. Solid line, upper two-impurity positive resonance energy; dashed line, lower two-impurity resonance energy; upper dashed-dotted line, reference one-impurity resonance energy $\Omega^+_0(V_0)$. Lower dashed-dotted line, one-impurity resonance energy for double-impurity strength $\Omega^+_0(2V_0)$. Symbol indicates resonant channel, $\circ=\Omega^+_1>0$; $\star=\Omega^+_2>0$.

where

$$\hat{M}_p=\begin{pmatrix} \mathcal{D}_2^+\mathcal{D}_1 & G_1(R,\omega)V_0\mathcal{D}_1 \\ G_1(R,\omega)V_0\mathcal{D}_1 & -\mathcal{D}_2^-\mathcal{D}_1 \end{pmatrix},$$

$$\hat{M}_s=\begin{pmatrix} \mathcal{D}_1^+\mathcal{D}_2 & -G_1(R,\omega)V_0\mathcal{D}_2 \\ -G_1(R,\omega)V_0\mathcal{D}_2 & -\mathcal{D}_1^-\mathcal{D}_2 \end{pmatrix}. \quad (14)$$

In certain special configurations, e.g., if the two impurities are located at 45° with respect to one other, it is easy to check that $G_1(\mathbf{R},\omega)=0\ \forall\ \mathbf{R}$. In this case the entire resonant denominator factorizes $\mathcal{D}=\mathcal{D}_{1+}\mathcal{D}_{1-}\mathcal{D}_{2+}\mathcal{D}_{2-}$. The T matrix then takes the simple diagonal form

$$\hat{T}_{\mathbf{k},\mathbf{k}'}(\omega)=2V_0\cos\left(\mathbf{k}\cdot\frac{\mathbf{R}}{2}\right)\cos\left(\mathbf{k}'\cdot\frac{\mathbf{R}}{2}\right)\left[\frac{\tau_+}{\mathcal{D}_{1-}}+\frac{\tau_-}{\mathcal{D}_{1+}}\right]$$
$$+2V_0\sin\left(\mathbf{k}\cdot\frac{\mathbf{R}}{2}\right)\sin\left(\mathbf{k}'\cdot\frac{\mathbf{R}}{2}\right)\left[\frac{\tau_+}{\mathcal{D}_{2-}}+\frac{\tau_-}{\mathcal{D}_{2+}}\right], \quad (15)$$

where $\tau_\pm\equiv(\tau_3\pm\tau_0)/2$.

IV. BOUND-STATE ENERGIES FOR TWO IMPURITIES

Measuring bound-state energies of impurity resonances in STM experiments allows one to obtain information on impurity potentials, and has the virtue of being independent of the STM tunneling matrix elements. On the other hand, resonance energies of isolated single impurities provide no information on the spatial structure of resonant or extended state electronic wave functions. In principle, measurement of only the resonance energies of isolated pairs of impurities with different separations $\mathbf{R}$ is the simplest method of getting spatially resolved information on electronic wave functions independent of the exact tunneling mechanism.

When two identical impurities with resonance energies Ω^-_0,Ω^+_0 are brought together, the bound-state wave functions interfere with one another, in general splitting and shifting each resonance, leading to four resonant frequencies $\Omega^-_1,\Omega^+_1,\Omega^-_2$, and Ω^+_2, where the subscript indicates which factor in Eq. (11) is resonant. If splittings are not too large, the electron and hole resonances are related in a similar way as in the one-impurity problem, $\Omega^-_1\simeq-\Omega^+_1$ and $\Omega^-_2\simeq-\Omega^+_2$. Again the weight of each resonance may be quite different or even zero on any given site. A large splitting may be taken as evidence for strong hybridization of quasiparticle wave functions. If we take the interimpurity distance R as a parameter and keep impurity potentials and other parameters fixed, there are two obvious limits where this splitting vanishes. In the case of separation $R=0$, the two impurities combine (mathematically) to create a single impurity of strength $2V_0$, so both $\Omega^\pm_{1,2}$ approach the $\Omega^\pm_0(2V_0)$ appropriate for the double-strength potential. In the case of infinite separation $R\to\infty$, we must find $\Omega^+_{1,2}$ approaching the $\Omega_0(V_0)$ appropriate for isolated single impurities.

A. Gas model

Equation (9) is a general result for two δ-function potentials embedded in a host described by an arbitrary G_0. We would like to derive analytical results for the resonance energies obtained therefrom to get some sense of the appropriate length scales and symmetries in the problem. At large distances, the resonance energies must approach the single impurity values, so the splittings can be calculated perturbatively. To do so one must first obtain analytical expressions for the large-distance behavior of the unperturbed Green's functions. This is difficult for the superconducting lattice tight-binding model on which most of this work is based, but much insight can be gained by studying the equivalent gas model, with spectrum $\epsilon_{\mathbf{k}}=\mathbf{k}^2/2m$. In this case expressions

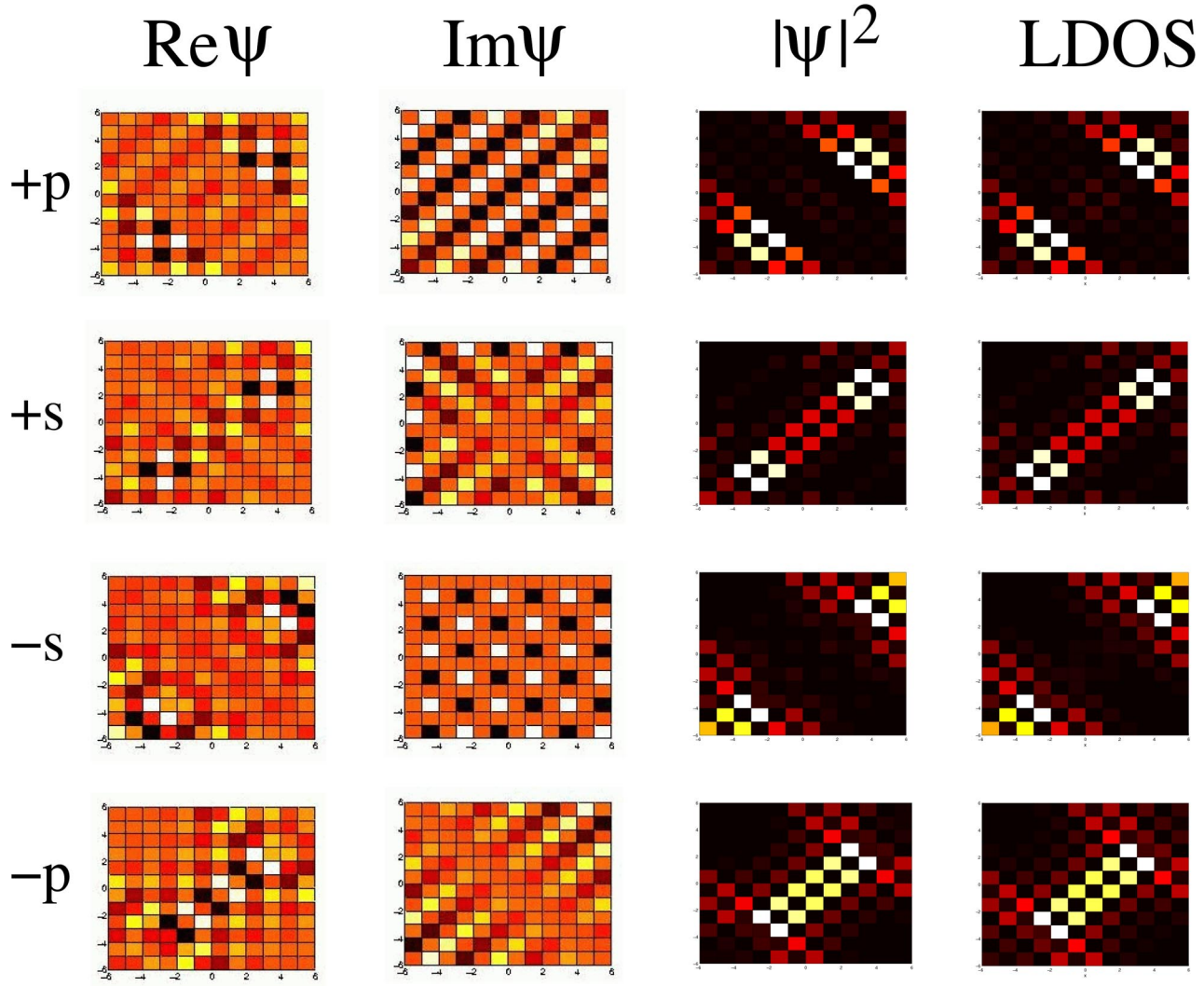

FIG. 4. (Color online) Comparison of symmetric (s) and antisymmetric (p) combinations of one-particle wave functions with exact LDOS for $\Delta_0=0.1$, $V_0=10$, $\mu=0$, $\mathbf{R}=(6,6)$. Two-impurity resonance energies are $\Omega_{2\pm}/t=\pm 0.0195$, $\Omega_{1\pm}/t=\pm 0.0075$. Energies are always ordered from highest (top) to lowest (bottom).

have been obtained by Joynt[34] and Balatsky *et al.*,[16] for the d-wave integrated Green's functions $G_\alpha(\mathbf{R},\omega)$ at large distances, both for $\mathbf{R}$ making an angle 45° or 0° with the x axis. For frequencies $\omega/\Delta_0 \ll 1/k_F r \ll 1/k_F\xi_0$, these reduce to

$$\hat{G}^0(\mathbf{R},\omega) \approx \begin{cases} N_0 \dfrac{e^{ik_F R}}{k_F R}\dfrac{k_F\xi_0}{4+\pi^2\xi_0^2 k_F^2}\tau_3 & \mathbf{R}\|(110) \\ N_0 \dfrac{e^{-R/\xi_0}}{\sqrt{k_F R}}\left[\left(i\dfrac{\omega}{\Delta_{max}}\tau_0+\tau_1+\tau_3\right)\cos k_F R \right. & \\ \left. \quad +\left(i\dfrac{\omega}{\Delta_{max}}\tau_0+\tau_1-\tau_3\right)\sin k_F R\right], & \mathbf{R}\|(100) \end{cases} \tag{16}$$

where $\xi_0=v_F/\pi\Delta_{max}$ is the coherence length.

The resonance energies may now be found by inserting these expressions for frequencies $\omega=\Omega_0^{\pm}+\delta$ into Eq. (9) and solving for the shifts δ. We find $\Omega_{1,2}^{+}\simeq\Omega_0^{+}\pm\delta$, with

$$\frac{\delta}{\Delta_{max}} \approx \begin{cases} \dfrac{1}{\ln(\Omega_0/\Delta_{max})}\dfrac{\sin k_F R}{k_F R}\dfrac{k_F\xi_0}{4+\pi^2\xi_0^2 k_F^2}, & \mathbf{R}\|(110) \\ \dfrac{e^{-R/\xi_0}}{\sqrt{k_F R}\ln(\Omega_0/\Delta_{max})}\cos(k_F R+\pi/4), & \mathbf{R}\|(100). \end{cases} \tag{17}$$

These expressions are valid for $\delta/\Omega_0^{+}\ll 1$.

Clearly the decay of the splitting $\sim\exp -r/\xi_0/\sqrt{k_F r}$ is much more rapid for distances larger than the coherence length along the antinode (100) than for along the nodes, where it falls as $\sim 1/r$. The lack of a scale in the long-distance interference of quasiparticle wave functions oriented along (110), where they strongly overlap, is of potentially

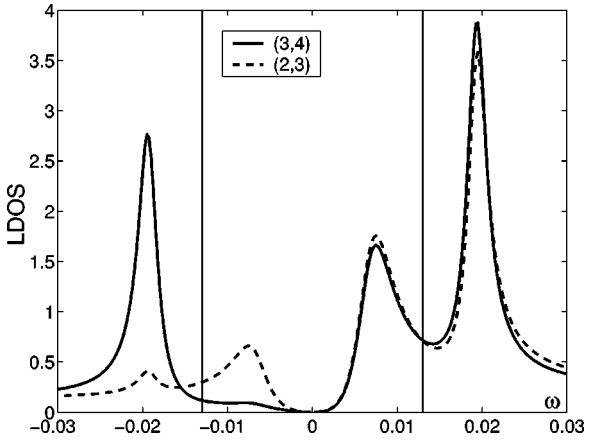

FIG. 5. Comparison of LDOS spectra $\rho(\mathbf{r},\omega)$ for various $\mathbf{r}$ with two impurities with $\Delta_0=0.1$, $V_0=10$, $\mu=0$ at positions $(-3,-3)$ and (3,3) [$\mathbf{R}=(6,6)$]. Vertical lines correspond to one-impurity resonances at $\Omega_0^{\pm}=\pm 0.013$. Note difference in vertical scales between upper and lower panels.

crucial importance in the STM analysis of ''isolated'' impurities, and we will bear this question in mind in what follows.

B. Lattice model

Here we consider a tight-binding model for ease of numerical evaluation. The definition of the resonant energies can be obtained either by finding the minimum of Eq. (9) or from an analysis of phase shifts.[35] The solutions corresponding to each factor in Eq. (10) can then, in general, be tracked as a function of separation R by minimizing $\mathcal{D}_{1,2}$ separately. In practice, this works well except in some special cases where the minima are very shallow. In Fig. 2 we show the result for a particle-hole symmetric system. It is seen that each factor $\mathcal{D}_\alpha$ corresponds to an oscillating function of R, with the factor determining, e.g., Ω_2^+, changing from site to site according to whether the site is even or odd. This is due to the strong R dependence of the components G_α; in the simplest case, $\mathbf{R}\|(110)$ and $\mu=0$, $G_3(\mathbf{R},\omega)=G_1(\mathbf{R},\omega)=0$, but $G_0(\mathbf{R},\omega)\equiv\Sigma_{\mathbf{k}}\cos(k_xR/\sqrt{2})\cos(k_yR/\sqrt{2})\,G^0_{\mathbf{k}}(\omega)$ oscillates rapidly. At $R=0$, the problem reduces to the double-strength single-impurity case; the factor $\mathcal{D}_1$ gives the resonant frequency $\Omega_0^{\pm}(2V_0)$ and the factor $\mathcal{D}_2$ is 1. At large separation the Ω_1^+ and Ω_2^+ ''envelopes'' are seen to converge to $\Omega_0^+(V_0)$ with a length scale of a few $\xi_0\simeq 10a$ for the parameters chosen.

In the $\mathbf{R}\|(100)$ case, the oscillations of the bound-state energies with increasing R are not so simple, as seen in Fig. 3. The one obvious simple difference from the (110) case is that the energy splittings vanish much faster with distance, as expected from the discussion in Sec. IV A. Otherwise the short-distance behavior of the bound-state energies is complicated. One can check that the energy closest to the Fermi level is Ω_2^+ when $R=2+4n$, n integer, and Ω_1^+ otherwise.

In general, the short-distance behavior is difficult to analyze analytically and we note that in neither the (110) nor (100) directions do resonances appear *at all* for $R=1$. Clearly the hybridization is so strong in these cases that the picture of perturbatively split one-impurity states breaks down. More importantly, the splittings are significant out to quite large distances. Parameters in Figs. 2 and 3 are chosen such that $\xi_0\approx 10a$, as seen from Fig. 3, where we indeed expect a e^{-R/ξ_0} falloff according to the preceding section. On the other hand, Fig. 2 indicates strong interference out to distances of $30a$ or more!

V. LOCAL DENSITY OF STATES

A. General

The spatial distribution of two-impurity bound-states gives much more detailed information about the nature of the quantum interference processes between impurities than the bound-state energies by themselves. Here we ask whether one can simply express the bound-state wave functions of the two-impurity system in terms of the one-impurity bound-states, and how they can be classified by symmetry. We would like to make predictions for STM experiments, including which qualitative features of the spectra reflect the quantum numbers of these states directly, and how these features depend on impurity potential and configuration. As indicated in the preceding section, it is important to determine how far apart two impurities need to be considered ''isolated.'' Finally, we would like to understand how robust these predictions are with respect to changes in band structure, scattering potential, etc.

Throughout this work, the LDOS refers to the *tunneling* density of states,

$$\rho(\mathbf{r},\omega)=\frac{1}{2}\sum_\sigma \rho_\sigma(\mathbf{r},\omega) \tag{18}$$

with the spin-resolved LDOS,

$$\rho_\uparrow(\mathbf{r},\omega)=-\pi^{-1}\mathrm{Im}G_{11}(\mathbf{r},\mathbf{r},\omega+i0^+), \tag{19a}$$

$$\rho_\downarrow(\mathbf{r},\omega)=+\pi^{-1}\mathrm{Im}\,G_{22}(\mathbf{r},\mathbf{r},-\omega-i0^+), \tag{19b}$$

where the subscripts 11 and 22 refer to the electron and hole parts of the diagonal Nambu Green's function.

The factor of 1/2 in Eq. (18) ensures that the LDOS normalization is

$$\int_{-\infty}^{\infty} d\omega\rho(\mathbf{r},\omega)=1.$$

Provided the peaks in the LDOS are well defined, the peak energies agree closely with the resonance energies defined by Eq. (4a). Some care is required, however, because peaks in the LDOS may not appear on all sites, and can be difficult to resolve. It is also worth noting that the peaks in the LDOS are not symmetric with respect to the Fermi energy, though in practice the degree of asymmetry is very small.

The local electron density of states measured by STM is given by Eq. (18), with

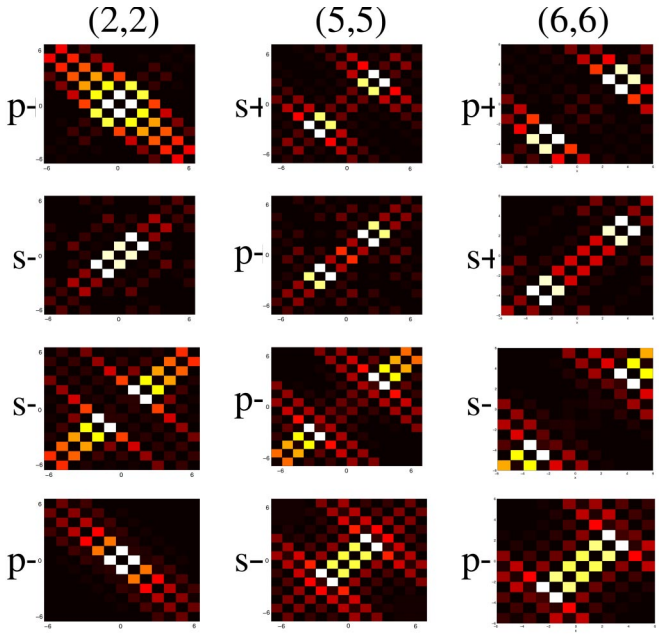

FIG. 6. (Color online) LDOS maps at resonant energies for $\mathbf{R}\|(110)$. Tight-binding band, $\Delta_0=0.1$, $V_0=10$, $\mu=0$.

$$\hat{G}(\mathbf{r},\mathbf{r},\omega)=\sum_{\mathbf{k}}\hat{G}^0(\mathbf{k},\omega)+\sum_{\mathbf{k},\mathbf{k}'}e^{-i(\mathbf{k}-\mathbf{k}')\cdot\mathbf{r}}\times\hat{G}^0(\mathbf{k},\omega)\hat{T}_{\mathbf{k}\mathbf{k}'}(\omega)\hat{G}^0(\mathbf{k}',\omega), \tag{20}$$

and $\hat{T}_{\mathbf{k}\mathbf{k}'}$ is the T matrix for any number of impurities.

B. Interference of one-impurity wave functions.

In the one-impurity case, the T matrix is given by Eq. (2) and it is easy to see that

$$-\delta G_{11}''(\mathbf{r},\mathbf{r},\omega)=-V_0\ \mathrm{Im}\left(\frac{[G_{11}^0(\mathbf{r})]^2}{S_-}+\frac{[G_{21}^0(\mathbf{r})]^2}{S_+}\right). \tag{21}$$

Quite generally one can express Green's function in terms of the exact eigenstates $\psi_n(\mathbf{r})$ of the system in the presence of the impurity[37]

$$\delta G_{11}(\mathbf{r},\mathbf{r},\omega)=\sum_n\frac{\psi_n^*(\mathbf{r})\psi_n(\mathbf{r})}{\omega-\Omega_n+i0^+}\approx\frac{\psi_n^*(\mathbf{r})\psi_n(\mathbf{r})}{\omega-\Omega_n}, \tag{22}$$

where the final approximation is valid for a true bound-state with ω very close to a particular bound-state energy Ω_n, and will be a good approximation in the present case to the extent the resonances are well defined, in the sense discussed above. Comparing with form (21) thus allows us to identify the positive- and negative-energy wave functions of the single-impurity resonances ($V_0>0$ assumed):

$$\psi_\pm(\mathbf{r})=Z_\pm\begin{cases}G_{21}^0(\mathbf{r},\omega), & \omega=\Omega_0^+\\ G_{11}^0(\mathbf{r},\omega), & \omega=\Omega_0^-,\end{cases} \tag{23}$$

where $Z_\pm$ are nonresonant wave function normalization factors. Note that the electronlike bound-state eigenfunction is directly related to the off-diagonal bare Green's function, while the holelike wave function is proportional to the diagonal bare Green's function.

We can follow the same procedure for the two-impurity Green's function, and ask how the eigenfunctions at a particular resonant energy are related to the single-impurity wave functions we have just found. Since the single-impurity resonant energies are different from the two-impurity energies, this analysis will be valid to the extent the splittings are small compared to $\Omega_{0\pm}$. The Green's function $\delta G(\mathbf{r},\mathbf{r})$ can now be constructed from Eq. (13) and the wave functions read off by comparing with the spectral representation in the same way as in the one-impurity case. By examining Eq. (13) it may be shown that, depending on whether $\mathcal{D}_1$ or $\mathcal{D}_2$ is resonant, the wave functions thus extracted will be of definite spatial parity, $\psi_n(\mathbf{r})=\pm\psi_n(-\mathbf{r})$. We find

$$\psi_+^p=Z_+^p\left(G_{11p}^0+\frac{G_1(\mathbf{R})V_0}{\mathcal{D}_2^+}G_{12p}^0\right),\quad \omega=\Omega_{2+},$$

$$\psi_-^p=Z_-^p\left(G_{11p}^0-\frac{\mathcal{D}_2^-}{G_1(\mathbf{R})V_0}G_{12p}^0\right),\quad \omega=\Omega_{2-},$$

$$\psi_+^s=Z_+^s\left(G_{11s}^0-\frac{G_1(\mathbf{R})V_0}{\mathcal{D}_1^+}G_{12s}^0\right),\quad \omega=\Omega_{1+},$$

$$\psi_-^s=Z_-^s\left(G_{11s}^0+\frac{\mathcal{D}_1^-}{G_1(\mathbf{R})V_0}G_{12s}^0\right),\quad \omega=\Omega_{1-}, \tag{24}$$

where $\hat{G}_{(s,p)}^0\equiv\hat{G}^0(\mathbf{r}-\mathbf{R}/2)\pm\hat{G}^0(\mathbf{r}+\mathbf{R}/2)$, and the $Z_\pm^{s,p}$ are normalization coefficients. These are the two-impurity odd (p) and even-parity (s) resonant state eigenfunctions expressed directly as linear combinations of the corresponding one-impurity eigenfunctions $\psi_\pm$ given in Eq. (23).

1. $\mathbf{R}\|(110)$

We note now that, in general, particle and holelike one-impurity eigenfunctions are mixed in each two-impurity state (24); this is possible because anomalous scattering processes with amplitude $G_1(\mathbf{R})$ can take place. There are special situations, including all configurations with $\mathbf{R}\|(110)$, where $G_1(\mathbf{R})=0$ and the eigenfunctions become much simpler and do not mix particle and hole degrees of freedom,

$$\psi_\pm^s(\mathbf{r})=Z_\pm^s\begin{cases}G_{21s}^0(\mathbf{r},\omega), & \omega=\Omega_{1+}\\ G_{11s}^0(\mathbf{r},\omega), & \omega=\Omega_{1-},\end{cases} \tag{25}$$

and

$$\psi_\pm^p(\mathbf{r})=Z_\pm^p\begin{cases}G_{21p}^0(\mathbf{r},\omega), & \omega=\Omega_{2+}\\ G_{11p}^0(\mathbf{r},\omega), & \omega=\Omega_{2-}.\end{cases} \tag{26}$$

We study this case now both to get a simple idea of how the quantum interference between two impurities works in practice, and because the (110) states are claimed to be of particular importance for the formation of the impurity band due to the strong interference of long-range tails in the quasiparticle wave functions. In Fig. 4, we have exhibited the

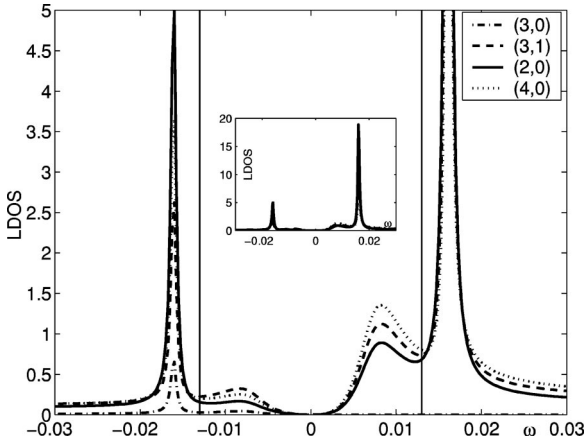

FIG. 7. Comparison of LDOS spectra $\rho(\mathbf{r},\omega)$ for various $\mathbf{r}$ with two impurities at positions $(-3,0)$ and $(3,0)$ $[\mathbf{R}=(6,0)]$. Tight-binding band, $\Delta_0=0.1$, $V_0=10$, $\mu=0$.

resonant state wave functions $\psi_{\pm}^{s,p}$ for the (110) case. We exhibit both the wave functions themselves, so that the reader may verify the parity of these states explicitly, and their absolute square. There is good agreement between the spatial pattern of the $|\psi|^2$ as defined and the exact LDOS calculated from Eq. (21) at each resonant energy, implying that near each resonant energy the nonresonant contributions are quite insignificant. It is clear that some states involve constructive and some destructive interference between the one-impurity wave functions in different regions of space, but the spatial patterns are, not unexpectedly, considerably more intricate than the ''hydrogen molecule'' type states one might first imagine would form, with electrons living either directly between impurities or completely expelled from this region. This is of course due to the *d*-wave character of the medium in which the quasiparticles propagate. For example, the LDOS is zero at the point halfway between the two impurities for the *p*-wave states, but it is quite small in the *s*-wave states as well. It is furthermore clear from the figure that both *s* and *p* functions can have either constructive or destructive character, in the molecular sense. Note that the states are shown arranged vertically according to their eigenenergies, but recall that the ordering of the *s* and *p* ($\mathcal{D}_1$ and $\mathcal{D}_2$) states changes according to whether *R* is even or odd, as indicated in Fig. 2.

In Fig. 5, we show the full energy variation of the LDOS spectra on sites near one of the impurities to illustrate the expected widths of the resonances and the variability with position. Note the surprisingly sharp high-energy resonances, which we discuss further below. On the other hand, on certain sites in the configuration of Fig. 5 such as (0,0), (2,2) and (4,4), virtually no LDOS weight at all is observed. In Fig. 6, we show LDOS maps for several impurity separations along (110). Note that in the high-energy *p* states for $\mathbf{R}=(2,2)$ and (6,6), both of which are fairly narrow, nearly total destructive interference exists along the (110) direction outside of the two impurities, but there is substantial weight along the $(1\bar{1}0)$ direction relative to each of the two impurities. As one moves the impurities apart, the tails of these wave functions in the $(1\bar{1}0)$ direction simply shift with the impurities. This suggests that these states may be somewhat narrowed, because the quasiparticle is localized between the two impurities, but only in the (110) direction; it may easily leak out along the $(1\bar{1}0)$ tails.

2. $\mathbf{R}\|(100)$

We noted above that for large separations the interference between quasiparticle wave functions vanishes much more rapidly with increasing separation in configurations with impurities aligned along a crystal axis $R\|(100)$. For small or intermediate spacings $R\lesssim\xi_0$, however, the bound-state splittings are just as large. Figure 7 shows a spectrum for impurities separated by six lattice constants in the (100) direction. Although the low-energy peaks are weak, there are, nevertheless, four well-defined peaks as expected. The most striking feature of Fig. 7 is that the upper resonance is extremely sharp, far sharper in fact than a single-impurity resonance at the same energy! This is counterintuitive based on our knowledge of the one-impurity problem: the *T*-matrix denominator $S_{\pm}$ defined in Eq. (2) has an imaginary part proportional to the density of states of the clean *d*-wave superconductor, so that the resonance width depends (approximately) linearly on the resonance energy. This is clearly not the case here. In the two-impurity problem where one impurity is at the origin and the second is at $\mathbf{R}$, the *T*-matrix denominator is given by Eq. (9), which can equivalently be written as

$$\mathcal{D}=\det[V_0^{-1}\tau_3-\hat{G}^{(1imp)}(\mathbf{R},\mathbf{R},\omega)]\det\hat{T}(\omega),$$

where $\hat{T}$ is the one-impurity *T* matrix and $\hat{G}^{(1imp)}$ is Green's function with one impurity at the origin. Thus sharp two-impurity resonances occur for exactly the same reason as in the one-impurity case, but because the one-impurity DOS at $\mathbf{R}$ is nonmonotonic in ω, the resonance broadening is not necessarily proportional to the resonance energy.

It seems intuitively clear that, because of destructive interference along the nodal directions, two-impurity bound-states *could* be formed in which quasiparticles are quite effectively trapped because they will be prevented from escaping via the long (110) tails of the individual impurity wave functions. In Fig. 8, the spatial structure of the high-energy states confirms our intuition, since quasiparticles appear to be confined primarily to the axis joining the impurities. The 45° tails of these two-impurity states are supressed in all directions, and as expected the spectral features are even narrower than for the $\mathbf{R}\|(110)$ configurations of Fig. 5. In the $\mathbf{R}=(2,0)$ case, the quasiparticle is nearly completely confined to the site between the two impurities, while the wave function spreads out somewhat in the $\mathbf{R}=(6,0)$ case. For these cases, $G_1(\mathbf{R},\omega)$ vanishes as in the (110) case, so the wave functions have the same structure as in Eqs. (25) and (26). We note that when the peaks are sharp, the resonance state is essentially localized, that is the contribution to the wave function at resonance from the continuum has vanishing weight. In general, one might have expected these states to decay as $1/r$ along the (110) direction and exponen-

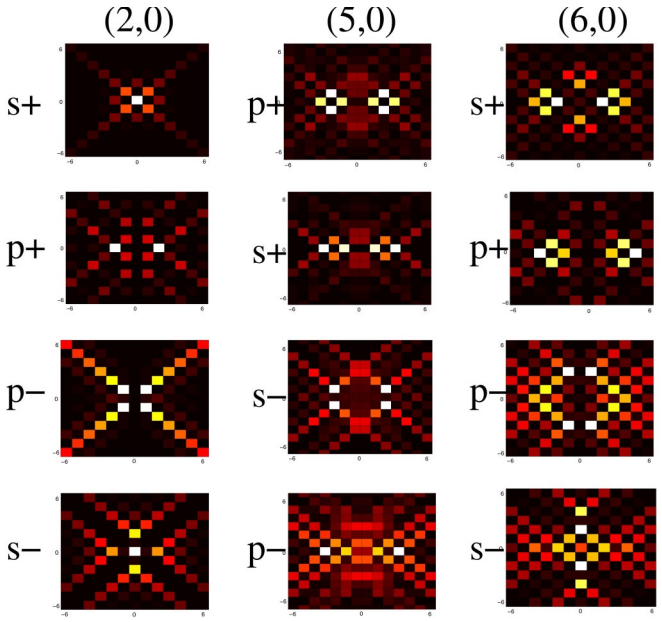

FIG. 8. (Color online) LDOS maps at resonant energies for $R\|(100)$. Tight-binding band, $\Delta_0=0.1$, $V_0=10$, $\mu=0$.

tially along the (100) direction, but they may decay more rapidly from interference effects.

Thus far we have considered only a simple tight-binding band at half-filling, and one might worry that the existence of quasilocalized states was a consequence of the perfect nesting of this special electronic structure, and that such features are unlikely to be observed in real systems. We show below that this is not the case, and argue that a commensuration of dominant scattering wave vectors *at the bound-state energy* is the important quantity, and that finding such a state depends on band structure and other details.

VI. REALISTIC BANDS

Until now we have focussed on the rather artificial symmetric tight-binding band case, both for calculational simplicity and to illuminate the unusual density of states phenomena driven by nesting features of the Fermi surface. Some, but clearly not all of these phenomena will survive away for a realistic band with particle-hole asymmetry. Because of the intense current interest on STM studies of the cuprates, we now focus exclusively on a ''realistic'' representation of the electronic structure of BSCCO-2212, which we parametrize by adopting the tight-binding coefficients of Norman *et al.*,[33]

$$\epsilon(k)=t_0+2t_1[\cos(k_x)+\cos(k_y)]+4t_2\cos(k_x)\cos(k_y)+2t_3[\cos(2k_x)+\cos(2k_y)]+2t_4[\cos(2k_x)\cos(ky)+\cos(k_x)\cos(2ky)]+4t_5\cos(2kx)\cos(2ky) \quad (27)$$

with $t_0,\ldots,t_5=0.879,-1,0.275,-0.087,-0.1876,0.086$ and $|t_1|\equiv 0.1488$ eV. The density of states of this band in both normal and superconducting states is shown in Fig. 9.

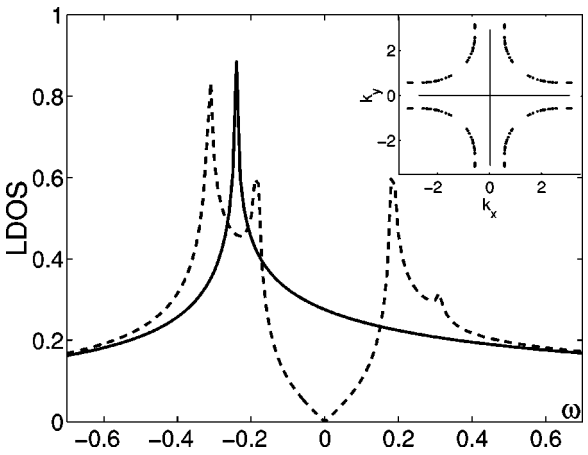

FIG. 9. Solid line, BSCCO total density of states after Ref. 33 vs ω/t_1. Dashed line, with *d*-wave superconducting gap of magnitude $\Delta_0=0.1t_1$. Insert, Fermi surface at optimal doping.

A. Direct spectra

We first reconsider some of the impurity configurations we treated in Sec. V to see how the LDOS patterns and bound states are affected by the electronic structure. The upper panel in Fig. 10 shows the distribtion of spectral weight on nearby sites for a configuration with impurities at separation $\mathbf{R}=(6,6)$. Comparison with the half-filled tight-binding model case shown in Fig. 5 shows little qualitative change on nearby sites with respect to either peak positions, spectral weight or spatial distribution. On the other hand, comparison of LDOS maps in Figs. 6 and 11 show that the longer-range character of the holelike resonances has changed considerably. In other cases, particularly for small R, the changes are much more drastic. In particular, one does not generally see all four resonances, as also found by Morr and Stavropoulos.[18] This is particularly true for resonances with $\mathbf{R}\|(100)$, as illustrated in the lower panel of Fig. 10, where the *low-energy* resonances have completely disappeared on all sites investigated.

To give an impression of the systematics of impurity resonance dependence on separation in the realistic system, and the configurations in which certain resonances are overdamped, in Fig. 12 we present a series of plots of LDOS spectra on nearest-neighbor sites along the line joining the impurities for a range of separations with $\mathbf{R}\|(100)$ and (110) directions. The number of peaks in each spectrum is variable, and for the closer separations normally only two peaks are observed (no peaks are observed for separation 1!). As the impurities are moved farther apart, hybridization weakens and it becomes easier to observe the full complement of four resonances. It is also clear that the bound-state splittings for the realistic band are decaying faster in the (100) direction, but that this splitting has not disappeared even for separations as large as $R=13$. This suggests that even in relatively dilute impurity systems the assumption of isolated impurities used to analyze recent STM experiments may need to be reexamined.

We note further that extremely sharp states occur frequently, for both even and odd separations; clearly the commensurability condition depends sensitively on the details of

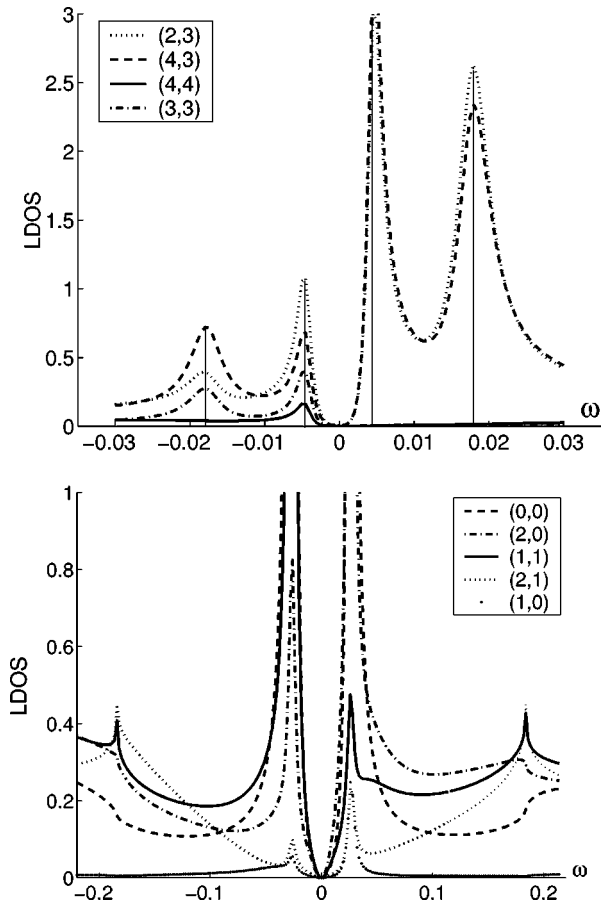

FIG. 10. LDOS spectra for various sites as indicated. Upper panel for impurities at (-3,-3) and (3,3) [$\mathbf{R}=(6,6)$], lower panel for impurities at (-1,0) and (1,0) [$\mathbf{R}=(2,0)$]. Parameters for "realistic" band (see text), energies ω in units of t_1, with $V_0=5.3$. Note peak at $\omega=-0.18$ in lower panel is gap edge, not impurity resonance.

the band structure. Contrary to the results of Ref. 18, we find that the state farthest from the Fermi level is frequently sharpest. In general, however, the spectra found here for the band of Ref. 33 are quite similar to those obtained in Ref. 18 when direct comparisons are possible.

The condition for a true bound-state [see Eq. (9)] is satisfied at frequency ω by $\hat{G}^0(\mathbf{R},\omega)\hat{T}\hat{G}^0(\mathbf{R},\omega)\hat{T}=1$. Since this must be satisfied independently for real and imaginary parts of $G^0(\mathbf{R},\omega)$, sharp resonances only appear for selected impurity separations. The product $\hat{G}^0(\mathbf{R},\omega)\hat{T}\hat{G}^0(\mathbf{R},\omega)\hat{T}$ in Eq. (9) is equivalently written as

$$\sum_{\mathbf{k},\mathbf{q}} e^{i\mathbf{q}\cdot\mathbf{R}}\hat{G}(\mathbf{k},\omega)\hat{T}(\omega)\hat{G}(\mathbf{k}+\mathbf{q},\omega)\hat{T}(\omega). \qquad (28)$$

It was argued by Hoffman *et al.*,[13] in an analysis of disordered BSCCO samples, that the characteristic wavevectors found in the spatial Fourier transform of the LDOS are determined by peaks in the joint density of states $\Sigma_{\mathbf{k}}\mathrm{Im}\,G_{11}(\mathbf{k},\omega)\mathrm{Im}\,G_{11}(\mathbf{k}+\mathbf{q},\omega)$. It is interesting to ask whether these same q-vectors are seen in Eq. (28).

At the small energies considered here, three distinct q vectors contribute to the joint DOS [a fourth, $q=0$ does not

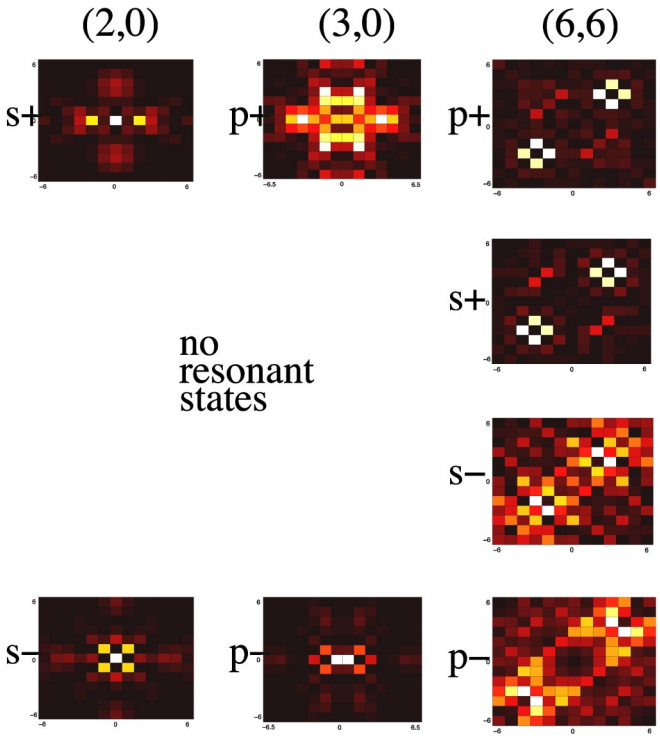

FIG. 11. (Color online) LDOS maps for realistic band (see text), $V_0=5.3t_1$.

produce any oscillatory $\mathbf{R}$ dependence in Eq. (28)], as illustrated in Fig. 13 (we neglect, for states sufficiently close to unitarity, the distinction between the tips of the quasiparticle constant energy contours and the nodal wave vectors). As a simple example, consider the realistic band model in the (100) direction, shown in the upper panel of Fig. 12. The $\mathbf{R}$ dependence of Eq. (28) is straightforward since $\mathbf{q}_1\cdot(1,0)=\mathbf{q}_2\cdot(1,0)\approx 2.28/a$, and $\mathbf{q}_3\cdot\mathbf{R}=0$, where a is the lattice constant. Naively, the standing-wave condition for a particle trapped between the two impurities is $(\mathbf{q}_1\cdot\mathbf{R}+2\eta_0)=n\pi$, where $\eta_0=\tan^{-1}(\pi N_0 V_0)$ is the one-impurity scattering phase shift. On the other hand, for $\mathbf{R}$ in the (110) direction, we must simultaneously satisfy the commensurability requirements $(\mathbf{q}_1\cdot\mathbf{R}+2\eta_0)=(\mathbf{q}_3\cdot\mathbf{R}+2\eta_0)=n\pi$, and $(\mathbf{q}_2\cdot\mathbf{R}+2\eta_0)=m\pi$ to form a resonant state, and we see that—as we observe in Fig. 12—sharp resonances occur much less frequently in the (110) than in the (100) direction. Quantitatively, the criterion for standing-wave formation is approximately satisfied for $\mathbf{R}=(3,0)$, (7,0), (11,0), (14,0) and $\mathbf{R}=(3,3)$, (11,11), which generally agrees with Fig. 12.

We stress, however, that the relative success of this naive picture at making quantitative predictions is a bit surprising. There is nothing in our consideration to account for the ω dependence of the T matrix, or for the Nambu structure of Green's functions. Furthermore, the approximation of the integral over $\mathbf{q}$ in Eq. (28) by a sum over a few dominant wave vectors is not expected to by justified at a quantitative level. Nonetheless, our considerations seem to indicate that the long-lived two-impurity bound-states are derived from a few selected wave vectors.

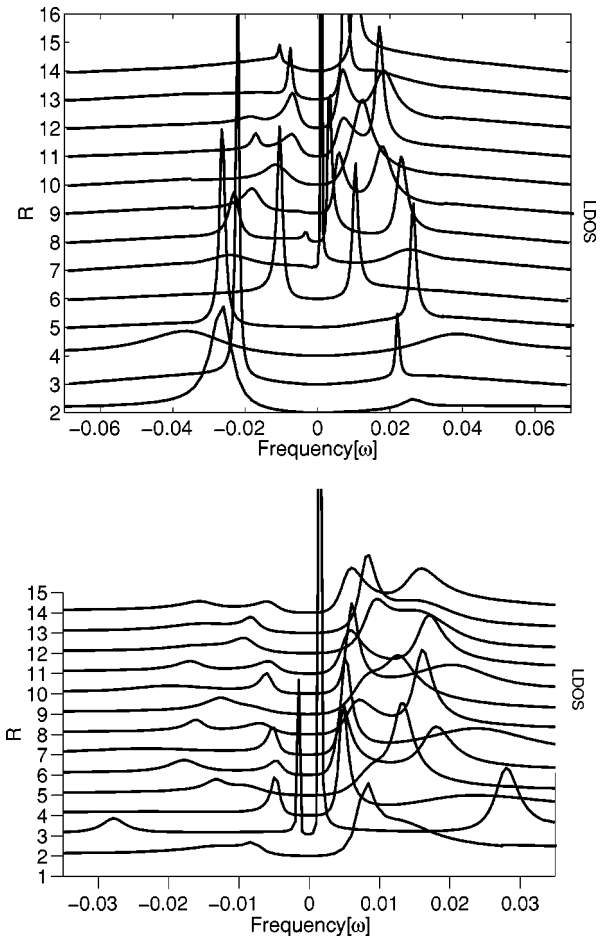

FIG. 12. LDOS spectra for realistic band and $V_0=5.3t_1$ on nearest-neighbor site. Upper panel, impurities at $(-R/2,0)$ and $(R/2,0)$ $[\mathbf{R}=(R,0)]$, spectra taken at $\mathbf{r}=(R/2,1)$. Lower panel, impurities at $(-R/2,-R/2)$ and $(R/2,R/2)$ $[\mathbf{R}=(R,R)]$, spectra taken at $\mathbf{r}=(R/2,R/2+1)$.

B. Filtering effects

The discrepancies between the simple picture of a Zn impurity as a strong potential scatterer in a *d*-wave superconducting host and the LDOS measured near Zn impurities in BSCCO-2212 samples have been alluded to above. Martin and Balatsky[16] proposed that this problem could be resolved by noting that electrons must first tunnel through the BiO layer before reaching the CuO_2 plane; applying the appropriate matrix elements for this process led them to a picture of a ''filtered'' DOS in which, in the simplest version, the STM tip samples not the LDOS corresponding to the atom directly under it, but rather to a sum of the LDOS on the surrounding four nearest-neighbor sites. With this ansatz, the LDOS pattern surrounding a Zn atom becomes, at a resonant energy of -1.5 meV, rather similar to the experimentally observed one, with a bright spot at the center of the pattern, see Fig. 14.

We now point out the rather obvious fact that this filtering mechanism is characteristic of the presence of the BiO layer in the BSCCO-2212 system, and should therefore be present in any STM measurement. If two nearby impurities are located via their resonant signals in such a measurement, the same filter should be applied to extract the true LDOS of the superconducting CuO_2 layer (see Fig. 15). *If* it is found that the filtering mechanism works only in the case of isolated impurities, but the observed pattern in the two-impurity case is quite different than that predicted by the simple filtered potential model, it must be abandoned and more sophisticated explanations sought. For example, it will be interesting to pursue the alternative ''Kondo'' explanation of Polkovnikov *et al.*,[19] in the case of the two-impurity problem. If one takes this model seriously, bringing two impurities close together should induce an RKKY interaction between the local moments on each impurity site, supressing the local Kondo screening and thereby weakening each impurity's scattering phase shift. One might then naively expect, in such a scenario, that bound-state energies would generally be found at higher energies than in the isolated impurity case. Of course, one's intuition based on the two-Kondo impurity problem in a normal metal is to be distrusted in this case, where the linear bare density of states already makes the one-impurity problem critical.[30]

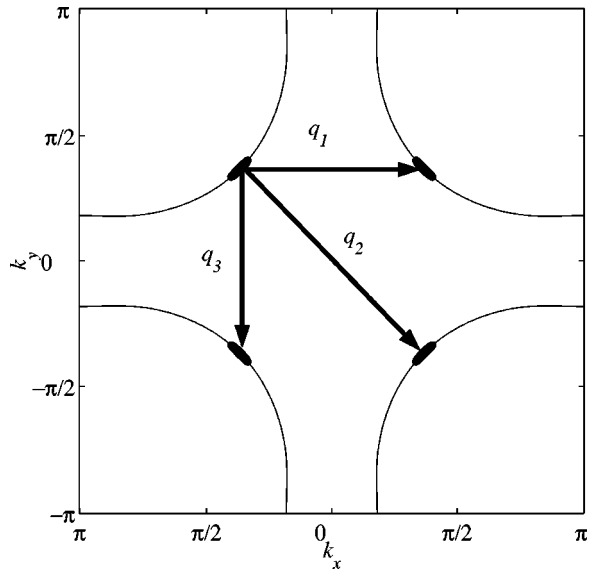

FIG. 13. Fermi surface of BSCCO-2212 with constant energy surfaces at $\omega=0.04$ shown as small filled ellipses at the nodal points. $\mathbf{q_1}$, $\mathbf{q_2}$, $\mathbf{q_3}$ are wave vectors for which the joint density of states is large.

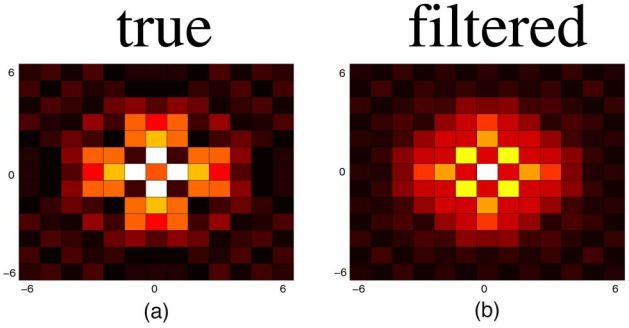

FIG. 14. (Color online) LDOS map for one strong repulsive impurity ($V_0=5.3$) at hole-type resonance $\Omega_0^-=0.011t_1$ in system with ''realistic band'' (see text) (a) without and (b) with filter.

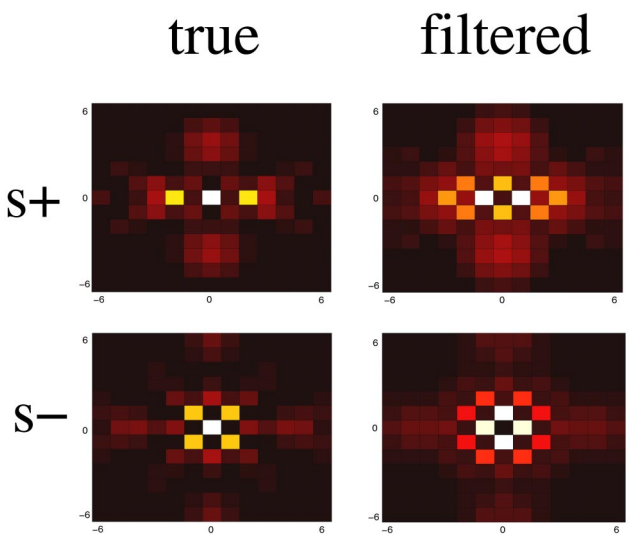

FIG. 15. (Color online) Comparison of true and filtered LDOS for two impurities at (-1,0) and (1,0), $\mathbf{R}=(2,0)$. $V_0=5.3$, $|\Omega_1^{\pm}|=0.026t_1$, ''realistic band'' (see text).

VII. CONCLUSIONS

In this paper we have explored a number of aspects of the quantum interference of impurity bound-states in *d*-wave superconductors. We gave the exact form of the two-impurity *t*-matrix for two potentials separated by **R**, and showed that, in general, it has four resonances at frequencies $\pm\Omega_1$ and $\pm\Omega_2$ which depend on **R**. In simple situations, the eigenfunctions of the two-impurity resonant states can be constructed explicitly in terms of the eigenfunctions of the one-impurity problem. Depending on the impurity configuration and electronic structure, some of the resonances are overdamped on specific sites or indeed sometimes over the entire lattice, leading to a smaller number of visible resonances in special situations. On the other hand, in other situations resonant states were observed in the two-impurity problem which were much sharper than their one-impurity counterparts, in some cases occuring quite far from the Fermi level, contradicting one's intuition that these states should be more strongly damped. We have interpreted these states as impurity ''traps'' in which quasiparticles are hindered by quantum interference, over surprisingly long lifetimes, from leaking out of the region between the two impurities.

The splitting of the bound-state energies relative to the one-impurity case was studied, and it was shown that the parity and energy of the two-impurity eigenfunctions oscillate as a function of impurity separation. At asymptotically large distances the splittings were shown to vary as $\sim 1/R$ for impurities aligned along the (110) direction and $\sim \exp(-R)/\sqrt{R}$ along (100). Systematic STM measurements of these splittings for isolated pairs of impurities at different **R** were shown to provide a direct measurement of spatial dependence of the Green's functions of the bulk superconductor.

Finally we calculated the local density of states for two impurities in a realistic band characteristic of the BSCCO-2212 system on which most STM experiments have been performed. The one qualitative difference relative to the particle-hole symmetric case we examined earlier was the overdamping of some bound-states on *any* lattice site we studied for certain impurity configurations. This makes it clear that even some qualitative features of LDOS spectra with two impurities will depend on details of the system in question. To extract information from STM when two-impurity configurations are isolated will therefore require a careful fit to theory. We have made predictions for several concrete situations which can be tested if such configurations can be found. In particular, we have calculated the density of states for realistic parameters corresponding to a Zn impurity in BSCCO, and given results for both the direct LDOS and for the ''filtered'' LDOS proposed by Martin and Balatsky[32] to explain discrepancies in the standard model of Zn as a potential scatterer when compared with experiment. If the ''filter'' works for isolated single Zn impurities but not for pairs of Zn atoms, it would be strong evidence in favor of an explanation for the Zn results in terms of residual induced local magnetism of the defect.

We close by remarking that the solution of the two-impurity problem may have important implications for the disordered *N*-impurity *d*-wave superconductor and the interpretation of STM experiments. In particular, we have shown on one hand that pairs of impurities can give rise to trapped states which have great deal of spectral weight; on the other hand, interference from other impurities can destroy the characteristic pattern expected for an ''isolated'' impurity even when they are widely separated. A more thorough investigation of these questions requires a careful comparison with the many-impurity system. One hint of the importance of the two-impurity states in the fully disordered system comes from the study of the perfectly nested band, where we find that many of the unusual symmetry-based features of the total density of states[38] are reflected already in the simple two-impurity problem as well. In addition, we have investigated the effects of self-consistent treatment of the order parameter on the results above, which were all produced assuming homogeneous $\Delta_{\mathbf{k}}$. We find that, although spectral weight is shifted by the order-parameter supression around the impurity site, in general away from the Fermi level,[39] the LDOS patterns are rather weakly affected. We will report in detail on these findings elsewhere.[35]

ACKNOWLEDGMENTS

This work was partially supported by NSF Grant Nos. NSF-DMR-9974396, BMBF 13N6918/1, and the Alexander von Humboldt Foundation. P.H. and L.Z. would also like to thank J. Mannhart and Lehrstuhl Experimentalphysik VI of the University of Augsburg for hospitality during preparation of the manuscript.

[1] J.M. Byers, M.E. Flatté, and D.J. Scalapino, Phys. Rev. Lett. **71**, 3363 (1993).
[2] A.V. Balatsky, M.I. Salkola, and A. Rosengren, Phys. Rev. B **51**, 15 547 (1995).
[3] P.C.E. Stamp, J. Magn. Magn. Mater. **63-64**, 429 (1987).
[4] See M.E. Flatté and J.M. Byers, Solid State Phys. **53**, 137 (1999).
[5] A. Yazdani, C.M. Howald, C.P. Lutz, A. Kapitulnik, and D.M. Eigler, Phys. Rev. Lett. **83**, 176 (1999).
[6] E.W. Hudson, S.H. Pan, A.K. Gupta, K-W. Ng, and J.C. Davis, Science **285**, 88 (1999); S.H. Pan, E.W. Hudson, K.M. Lang, H. Eisaki, S. Uchida, and J.C. Davis, Nature (London) **403**, 746 (2000).
[7] S.-H. Pan, J.P. O'Neal, R.L. Badzey, C. Chamon, H. Ding, J.R. Engelbrecht, Z. Wang, H. Eisaki, S. Uchida, A.K. Gupta, K.-W. Ng, E.W. Hudson, K.M. Lang, and J.C. Davis, Nature (London) **413**, 282 (2001).
[8] K.M. Lang, V. Madhavan, J.E. Hoffman, E.W. Hudson, H. Eisaki, S. Uchida, and J.C. Davis, Nature (London) **415**, 412 (2002).
[9] J.E. Hoffman, E.W. Hudson, K.M. Lang, V. Madhavan, H. Eisaki, S. Uchida, and J.C. Davis, Science **295**, 466 (2002).
[10] C. Howald, P. Fournier, and A. Kapitulnik, Phys. Rev. B **64**, 100504 (2001); C. Howald, H. Eisaki, N. Kaneko, A. Kapitulnik, cond-mat/0201546 (unpublished).
[11] D.P. Arovas, A.J. Berlinsky, C. Kallin, and S.-C. Zhang, Phys. Rev. Lett. **79**, 2871 (1997); Y. Chen and C.S. Ting, Phys. Rev. B **65**, 180513 (2002); J.-X. Zhu and C.S. Ting, Phys. Rev. Lett. **87**, 147002 (2001).
[12] E. Demler, S. Sachdev, and Y. Zhang, Phys. Rev. Lett. **87**, 067202 (2001); J.X. Zhu, I. Martin, and A. Bishop, *ibid.* **89**, 067003 (2002).
[13] J.E. Hoffman, K. McElroy, D.-H. Lee, K.M. Lang, H. Eisaki, S. Uchida, and J.C. Davis, Science **297**, 5584 (2002).
[14] Q.-H. Wang and D.-H. Lee, cond-mat/0205118 (unpublished).
[15] Y. Onishi, Y. Ohashi, Y. Shingaki, and K. Miyake, J. Phys. Soc. Jpn. **65**, 675 (1996).
[16] A.V. Balatsky and M.I. Salkola, Phys. Rev. Lett. **76**, 2386 (1996); see also D.N. Aristov and A.G. Yashenkin, *ibid.* **80**, 1116 (1998); A.V. Balatsky and M.I. Salkola, *ibid.* **80**, 1117 (1998).
[17] U. Micheluchi, F. Venturini, and A.P. Kampf, cond-mat/0107621 (unpublished).
[18] D. Morr and N. Stavropoulos, Phys. Rev. B **66**, 140508 (2002).
[19] Anatoli Polkovnikov, Subir Sachdev, and Matthias Vojta, Phys. Rev. Lett. **86**, 296 (2001).
[20] Kwon Park, cond-mat/0203142 (unpublished).
[21] G. Khalliulin, R. Kilian, S. Krivenko, and P. Fulde, Phys. Rev. B **56**, 11 882 (1997).
[22] M. Laukamp, G.B. Martins, C. Gazza, A.L. Malvezzi, E. Dagotto, P.M. Hansen, A.C. López, and J. Riera, Phys. Rev. B **57**, 10 755 (1998).
[23] H. Tsuchiura, Y. Tanaka, M. Ogata, and S. Kashiwaya, Phys. Rev. Lett. **84**, 3165 (2000); H. Tsuchiura, Y. Tanaka, M. Ogata, and S. Kashiwaya, Phys. Rev. B **64**, 140501 (2001).
[24] Jian-Xin Zhu and C.S. Ting, Phys. Rev. B **63**, 020506 (2001).
[25] Shi-Dong Liang and T.K. Lee, cond-mat/0206197 (unpublished).
[26] Ziqiang Wang and Patrick A. Lee, cond-mat/0205301 (unpublished).
[27] Anatoli Polkovnikov, Matthias Vojta, and Subir Sachdev, Phys. Rev. B **65**, 220509 (2002).
[28] J. Bobroff, H. Alloul, W.A. MacFarlane, P. Mendels, N. Blanchard, G. Collin, and J.-F. Marucco, Phys. Rev. Lett. **86**, 4116 (2001); **83**, 4381 (1999); A.V. Mahajan, H. Alloul, G. Collin, and J.F. Marucco, Eur. Phys. J. B **13**, 457 (2000); however, see also J.L. Tallon, J.W. Loram, and G.V.M. Williams, Phys. Rev. Lett. **88**, 059702 (2002); and J. Bobroff, W. A. MacFarlane, H. Alloul, and P. Mendels, *ibid.* **88**, 059702 (2002).
[29] M.-H. Julien, T. Fehér, M. Horvatić, C. Berthier, O.N. Bakharev, P. Ségransan, G. Collin, and J.-F. Marucco, Phys. Rev. Lett. **84**, 3422 (2000).
[30] Kevin Ingersent, Phys. Rev. B **54**, 11 936 (1996); C. Gonzalez-Buxton and K. Ingersent, *ibid.* **57**, 14 254 (1998).
[31] J.X. Zhu, C.S. Ting, and C.R. Hu, Phys. Rev. B **62**, 6027 (2000).
[32] I. Martin, A.V. Balatsky, and J. Zaanen, Phys. Rev. Lett. **88**, 097003 (2002).
[33] M.R. Norman, M. Randeria, H. Ding, and J.C. Campuzano, Phys. Rev. B **52**, 615 (1995).
[34] R. Joynt, J. Low Temp. Phys. **109**, 811 (1997).
[35] W.A. Atkinson, P.J. Hirschfeld, and L. Zhu (unpublished).
[36] W.A. Atkinson, P.J. Hirschfeld, and A.H. MacDonald, Physica C **341-348**, 1687 (2000).
[37] E.N. Economou, *Green's Functions in Quantum Physics*, 2nd ed. (Springer-Verlag, Berlin, 1983).
[38] A.G. Yashenkin, W.A. Atkinson, I.V. Gornyi, P.J. Hirschfeld, and D.V. Khveshchenko, Phys. Rev. Lett. **86**, 5982 (2001).
[39] W.A. Atkinson, P.J. Hirschfeld, and A.H. MacDonald, Phys. Rev. Lett. **85**, 3922 (2000).